Kannan N. Premnath[1,2]
Visiting Fellow
Mem. ASME
CUNY Energy Institute,
City College of New York,
City University of New York,
New York, NY 10031
e-mail: kannan.premnath@ucdenver.edu

Martin J. Pattison
HyPerComp Inc.,
2629 Townsgate Road,
Suite 105,
West Lake Village, CA 91361

Sanjoy Banerjee
CUNY Distinguished Professor
Mem. ASME
Director
CUNY Energy Institute,
Department of Chemical Engineering,
City College of New York,
City University of New York,
New York, NY 10031

An Investigation of the Lattice Boltzmann Method for Large Eddy Simulation of Complex Turbulent Separated Flow

Lattice Boltzmann method (LBM) is a relatively recent computational technique for fluid dynamics that derives its basis from a mesoscopic physics involving particle motion. While the approach has been studied for different types of fluid flow problems, its application to eddy-capturing simulations of building block complex turbulent flows of engineering interest has not yet received sufficient attention. In particular, there is a need to investigate its ability to compute turbulent flow involving separation and reattachment. Thus, in this work, large eddy simulation (LES) of turbulent flow over a backward facing step, a canonical benchmark problem which is characterized by complex flow features, is performed using the LBM. Multiple relaxation time formulation of the LBM is considered to maintain enhanced numerical stability in a locally refined, conservative multiblock gridding strategy, which allows efficient implementation. Dynamic procedure is used to adapt the proportionality constant in the Smagorinsky eddy viscosity subgrid scale model with the local features of the flow. With a suitable reconstruction procedure to represent inflow turbulence, computation is carried out for a Reynolds number of 5100 based on the maximum inlet velocity and step height and an expansion ratio of 1.2. It is found that various turbulence statistics, among other flow features, in both the recirculation and reattachment regions are in good agreement with direct numerical simulation and experimental data. [DOI: 10.1115/1.4023655]

1 Introduction

Turbulent flows involving separation and reattachment are common in many situations in nature and engineering systems. Examples of the latter include internal flow through diffusers and combustors and external flow past airfoils. Generally, the presence of an adverse pressure gradient causes flow separation and subsequent reattachment leading to the formation of a recirculating bubble. A canonical problem in this regard is the turbulent flow over a backward facing step. The geometric simplicity of this problem is contrasted by the complexity of flow features, including the boundary layer and free shear layer flows evolving into recirculation and reattachment regions. Owing to this, its numerical simulation is challenging and represents as an important benchmark problem for assessment of turbulence models and numerical schemes.

Early studies involving two-dimensional computations of flow over a backward facing step based on the solution of the Navier–Stokes (NS) equations at low Reynolds numbers were carried out by Armaly et al. (1993) [1], and Kaiktsis et al. (1991) [2]. For turbulent flows, large scales have most of the energy containing eddies that are specific to the flow configuration and the small scales that are generally more isotropic can be modeled. This forms the basis of the large eddy simulation (LES) technique, in which only the subgrid scales (SGS) are modeled [3]. On the other hand, the computation of all relevant turbulence scales without the use of models, i.e., the direct numerical simulation (DNS) provides full information at high computational costs; the use of Reynolds-averaged models, while resulting in a reduction in computational overhead, requires considerable empiricism. Thus, the LES approach represents a compromise between these two approaches. In the context of the backward facing step problem, Friedrich and Arnal (1990) [4] and Akselvoll and Moin (1993) [5] investigated the use of LES technique based on the NS equations. A detailed study involving DNS of turbulent flow over a backward facing step was performed by Le et al. (1997) [6]. They characterized the unsteady nature of this problem and presented a detailed structure of the turbulence statistics. This, together with a companion experimental study involving measurements by Jovic and Driver (1994) [7,8], provides the data for comparison and validation of the accuracy of numerical techniques.

Lattice Boltzmann methods (LBM), which evolved from the lattice gas cellular automata [9] as a physically and computationally improved version to a minimal discrete kinetic model of the Boltzmann equation [10], have emerged as an alternative computational method for fluid mechanics problems [11,12]. The solution of the lattice Boltzmann equation (LBE), a simplified form of the Boltzmann equation, is generally presented in terms of a stream-and-collide procedure, representing free-flight and relaxation process, respectively, of the distribution of particle populations. When the lattice, which represents the discrete directions for particle advection, has sufficient rotational symmetry, the LBE asymptotically recovers the weakly compressible NS equations. Direct connection to kinetic theory has resulted in improved physical modeling; for example, of multiphase [13,14] and multicomponent [15] flows and in an asymptotic theory for numerical analysis [16]. An important consideration in the LBM is the representation of the collision term. Owing to its simplicity, it is often represented by means of the single relaxation time (SRT) model [17], in which the distribution function for all discrete directions relax at the same rate [18,19]. On the other hand, the relaxation process due to collisions can more naturally be described in terms of an equivalent set of moments, which can, in general relax at different rates. This forms the basis of the multiple relaxation time (MRT) formulation [20–22]. By a careful choice of relaxation times based on a linear stability analysis, its numerical stability

[1]Corresponding author.
[2]Department of Mechanical Engineering, University of Colorado Denver, 1200 Larimer Street, Denver, CO 80217.

Contributed by the Fluids Engineering Division of ASME for publication in the JOURNAL OF FLUIDS ENGINEERING. Manuscript received March 24, 2012; final manuscript received January 9, 2013; published online April 3, 2013. Assoc. Editor: Ali Beskok.

 Copyright © 2013 by ASME

Downloaded From: https://fluidsengineering.asmedigitalcollection.asme.org on 06/30/2019 Terms of Use: http://www.asme.org/about-asme/terms-of-use

can be significantly enhanced as compared to the SRT-LBM [21]. The superior stability characteristics of the MRT-LBM has been demonstrated for various complex flows, including multiphase systems [23], magnetohydrodynamics [24], and turbulent flows [25]. Another important advantage of the MRT approach is the minimization of undesirable viscosity dependent discrete kinetic effects near walls by a careful parametrization of the relaxation times for the odd and even moments [26–29]. As a result of the algorithmic simplicity, amenability to parallelization with near-linear scalability, and its ability to represent complex boundary conditions and incorporate physical models more naturally, it has recently attracted considerable attention [30–36].

In particular, the LBM has been used for computational studies involving turbulent flows. Due to its kinetic origins, it has been analyzed for developing turbulence models from a more fundamental standpoint [37–39], and for simulations based on Reynolds-averaged description [40]. The LBM has been investigated for LES using the Smagorinsky eddy-viscosity SGS model [41] for simple turbulent flows based on the SRT [42] and MRT formulations [25,43,44], with a focus on wall-bounded flows using a damping function [45] in a multiblock approach in a recent study [25]. Other recent studies on the application of the LBM for turbulent flows include [46–49]. These works employed "constant" Smagorinsky-type SGS models, where the constant is obtained empirically and specified a priori, which limits its applicability to general flow situations. Furthermore, some of the studies (e.g., Ref. [48]) did not account for the need to damp the turbulence effects near walls, which can have important influence on the accuracy of results. It may be noted that some of the conclusions made in Ref. [49] regarding the lack of significant advantage of the MRT formulation vis-á-vis the SRT-LBM for turbulent flows is inconsistent with our prior findings (e.g., Ref. [25]), which demonstrated the superiority of the former approach for such problems. Other types of SGS models that have been investigated, such as in Refs. [46,47], may be useful for a class of problems but are still not without empiricism. To circumvent the above limitation, the dynamic procedure [50] has recently been extended for use with the LBM [51], which was further applied to flows with scalar transport such as heat transfer in a later study [52]. Based on the information of resolved scales, the model coefficient for the unresolved scales can be locally computed using this approach. Furthermore, it would also provide the correct near-wall limiting behavior self-consistently without the use of *ad hoc* wall functions, is able to handle transitional flows and does not rule out backscatter of energy to larger scales. Such a procedure becomes important for LES of complex turbulent flows, such as that over a backward facing step configuration, using the LBM.

In this work, we will study and assess the LBM for LES of a demanding problem involving turbulent flow over a backward facing step, characterized by complex flow features including separation and reattachment. It may be noted that prior work on LBM for the backward facing step problem is very limited, focusing particularly on low Reynolds number laminar flows (e.g., Ref. [53]). Hence, there is a great need to investigate the ability of the LBM for eddy-capturing simulations of such complex turbulent flows. Multiple relaxation time LBM formulation, which maintains numerical stability, is employed with multiblock grids that reduce computational overhead while resolving near-wall turbulence structures. Dynamic procedure is applied to the Smagorinsky SGS model to locally compute the model coefficient based on the resolved fluid motion. Appropriate inflow and outflow boundary conditions are employed to adequately maintain the relevant mean and turbulence motions at these boundaries. Simulations are performed for a Reynolds number of 5100 and an expansion ratio of 1.2, for which DNS [6] and experimental data [7] are available. The computed turbulence structure will be compared with these data to assess the LBM.

The paper is organized as follows. Section 2 briefly discusses the multiple relaxation time (MRT)-LBM. The dynamic procedure employed with the SGS model for representing unresolved motions is presented in Sec. 3. Section 4 provides a concise discussion of conservative locally refined multiblock gridding strategy. The problem specification, including the geometric configuration, boundary conditions, and computational conditions, is presented in Sec. 5. A comparison of turbulent statistics is made along with a discussion of results in Sec. 6. The main conclusions of this work are summarized in Sec. 7.

2 Multiple Relaxation Time Lattice Boltzmann Method

We will now briefly present the key elements of the MRT-LBM that allow incorporation of the Smagorinsky SGS model using the dynamic procedure. For details, the reader is referred to Refs. [22,25,44,51]. In the stream-and-collide depiction of the LBM, the collision process is represented as a relaxation of the distribution functions to their local equilibrium; the streaming step describes the advection of the distribution functions along the discrete characteristic directions represented by a lattice. The three-dimensional, nineteen particle velocity (D3Q19) lattice considered in this work is shown in Fig. 1, which corresponds to the particle velocity $\vec{e_\alpha}$ given by

$$\vec{e_\alpha} = \begin{cases} (0,0,0) & \alpha = 0 \\ (\pm 1,0,0),(0,\pm 1,0),(0,0,\pm 1) & \alpha = 1,\ldots,6 \\ (\pm 1,\pm 1,0),(\pm 1,0,\pm 1),(0,\pm 1,\pm 1) & \alpha = 7,\ldots,18 \end{cases} \tag{1}$$

The distinguishing feature of the MRT-LBM is that it computes collision in *moment space*, while the streaming process is performed in the usual *particle velocity space* [22]. For convenience, the following notations are used. The local distribution function $\mathbf{f}$ and its local equilibrium $\mathbf{f}^{eq}$ in *particle velocity space* may be written as the following column vectors: $\mathbf{f} = [f_0, f_1, f_2, \ldots, f_{18}]^\dagger$ and $\mathbf{f}^{eq} = [f_0^{eq}, f_1^{eq}, f_2^{eq}, \ldots, f_{18}^{eq}]^\dagger$, where the superscript † represents the transpose operator. The distribution functions $\mathbf{f}$ are transformed into equivalent moments $\hat{\mathbf{f}}$ through $\hat{\mathbf{f}} = \mathcal{T}\mathbf{f}$ where $\mathcal{T}$ is the transformation matrix. Here, and in the following, the "hat" represents the moment space. $\mathcal{T}$ is constructed such that the collision matrix in moment space $\hat{\Lambda}$ is a diagonal matrix, i.e., $\hat{\Lambda} = \mathcal{T}\Lambda\mathcal{T}^{-1}$, where Λ is the collision matrix in particle velocity space. This follows when $\mathcal{T}$ is orthogonal, which is formed from combinations of monomials of the Cartesian components of the particle velocity $\vec{e_\alpha}$ through the standard Gram–Schmidt procedure [22]. Furthermore, the equilibrium moments follow from $\hat{\mathbf{f}}^{eq} = \mathcal{T}\mathbf{f}^{eq}$. The components of the moment-projections of these quantities are: $\hat{\mathbf{f}} = [\hat{f}_0, \hat{f}_1, \hat{f}_2, \ldots, \hat{f}_{18}]^\dagger$ and $\hat{\mathbf{f}}^{eq} = [\hat{f}_0^{eq}, \hat{f}_1^{eq}, \hat{f}_2^{eq}, \ldots, \hat{f}_{18}^{eq}]^\dagger$, which are given in Appendix A for completeness.

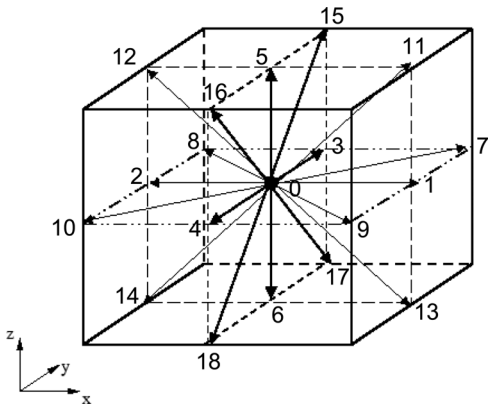

Fig. 1 Schematic illustration of the three-dimensional, nineteen velocity (D3Q19) model

Downloaded From: https://fluidsengineering.asmedigitalcollection.asme.org on 06/30/2019 Terms of Use: http://www.asme.org/about-asme/terms-of-use

The solution of the MRT-LBM can thus be written in terms of the following collision and streaming steps, respectively:

$$\tilde{\mathbf{f}}(\vec{x},t) = \mathbf{f}(\vec{x},t) + \Omega(\vec{x},t) \tag{2}$$

and

$$f_\alpha(\vec{x} + \vec{e}_\alpha \delta_t, t + \delta_t) = \tilde{f}_\alpha(\vec{x},t) \tag{3}$$

where the distribution function $\mathbf{f} = \{f_\alpha\}_{\alpha=0,1,\ldots,18}$ is updated due to collision resulting in the post-collision distribution function $\tilde{\mathbf{f}} = \{\tilde{f}_\alpha\}_{\alpha=0,1,\ldots,18}$ before being shifted along the characteristic directions during the streaming step. Ω represents the change in distribution function due to collisions as a relaxation process and is given by

$$\Omega(\vec{x},t) = \mathcal{T}^{-1}\left[-\hat{\Lambda}\left(\hat{\mathbf{f}}(\vec{x},t) - \hat{\mathbf{f}}^{eq}(\vec{x},t)\right)\right] \tag{4}$$

where $\hat{\Lambda} = \mathrm{diag}(s_0, s_1, \ldots, s_{18})$ is the diagonal collision matrix in moment space. Now, some of the relaxation times s_α, i.e., those corresponding to the hydrodynamic modes can be related to the transport coefficients and modulated by eddy-viscosity due to the SGS model as follows [22,25,44]: $s_1^{-1} = (9/2)\zeta + (1/2)$, where ζ is the molecular bulk viscosity, and $s_9 = s_{11} = s_{13} = s_{14} = s_{15} = s_\nu$, where $s_\nu^{-1} = 3(\nu/\Delta t) + (1/2) = 3[(\nu_0 + \nu_t)/\Delta t] + (1/2)$, with ν_0 being molecular shear viscosity and ν_t the eddy-viscosity determined from the dynamic SGS model discussed in Sec. 3. The rest of the relaxation parameters, i.e., for the kinetic modes, can be chosen through a linear stability analysis, as given in Ref. [22].

The hydrodynamic fields, i.e., the density ρ, velocity $\vec{u}$ and pressure p can then be obtained as follows:

$$\rho = \sum_{\alpha=0}^{18} f_\alpha, \quad \vec{j} \equiv \rho\vec{u} = \sum_{\alpha=0}^{18} f_\alpha \vec{e}_\alpha, \quad p = c_s^2 \rho \tag{5}$$

where $c_s = c/\sqrt{3}$ with $c = \delta_x/\delta_t$ being the particle speed, and δ_x and δ_t are the lattice spacing and time step, respectively. It follows from the Chapman–Enskog expansion that the MRT-LBM augmented by an eddy-viscosity recovers the "grid filtered" weakly compressible Navier–Stokes equations [23,54]. Thus, the density, momentum and pressure obtained from Eq. (5) are effectively grid-filtered quantities: $\rho \to \bar{\rho}, \rho\vec{u} \to \bar{\rho}\vec{\bar{u}}$ and $p \to \bar{p}$, where the "overbar" represents a quantity that is grid-filtered. Optimization procedures, based on the properties of $\mathcal{T}$, need to be fully exploited for an efficient implementation [22,25,44,51].

3 Subgrid Scale Model Using Dynamic Procedure

The use of the dynamic procedure for estimating the model coefficient of the SGS models at the grid-scale relies on sampling the smallest super-grid resolved scales (i.e., test-filtered scales), and assuming scale-invariance at these two levels [50]. If $\bar{\Delta}$ is the width of the grid-filter ($\bar{\Delta} = \delta_x$, where δ_x is the lattice grid spacing) and $\tilde{\bar{\Delta}}$ is the test-filter width, then a common choice is $\tilde{\bar{\Delta}}/\bar{\Delta} = 2$ [50]. Here, "bar" refers to the grid-filtered values and a "tilde" refers to the test-filtered values. The effect of unresolved turbulent motions at subgrid scales is parameterized by an eddy-viscosity model [41]

$$\nu_t = C\bar{\Delta}^2|\bar{S}| \tag{6}$$

where $|\bar{S}|$ is the strain rate, given by $|\bar{S}| = \sqrt{2\bar{S}_{ij}\bar{S}_{ij}}$ and C is the model coefficient. It follows from a Chapman–Enskog analysis that the grid-filtered strain rate $|\bar{S}|$ can be algebraically related to the local nonequilibrium moments, and direct velocity differencing can thus be avoided (see Appendix A). The main element involved, then, is the determination of the model coefficient C, which is accomplished as follows.

By invoking scale-invariance, the anisotropic part of the SGS stress at the grid-filter scale τ_{ij} ($\tau_{ij} = \bar{u}_i\bar{u}_j - \overline{u_iu_j}$) and that at the test-filter scale T_{ij} ($T_{ij} = \tilde{\bar{u}}_i\tilde{\bar{u}}_j - \widetilde{u_iu_j}$), where $\overline{u_iu_j}$ and $\widetilde{u_iu_j}$ are unknowns, are respectively modeled in terms of the above eddy-viscosity relations using the strain rates at corresponding scales. The unknown SGS stress at each filter level can then be related by the Germano identity [50] $L_{ij} = \widetilde{\bar{u}_i\bar{u}_j} - \widetilde{\bar{u}_i}\widetilde{\bar{u}_j} = T_{ij} - \tilde{\tau}_{ij}$, where L_{ij} is the resolved turbulent stress, a known quantity. Upon substituting the eddy-viscosity parameterizations on the right hand side of L_{ij}, an over determined system is obtained for the determination of the model coefficient C [50], which can be solved by a least square minimization approach [55] to yield

$$C = -\frac{1}{2}\frac{\langle L_{kl}M_{kl}\rangle}{\langle M_{ij}M_{ij}\rangle} \tag{7}$$

where

$$M_{ij} = \tilde{\bar{\Delta}}^2|\tilde{\bar{S}}|\tilde{\bar{S}}_{ij} - \bar{\Delta}^2\widetilde{|\bar{S}|\bar{S}_{ij}} \tag{8}$$

In Eq. (7), the usual summation convention of the repeated indices is assumed and $\langle\cdot\rangle$ represents spatial averaging in homogeneous directions or time averaging or both, depending on the problem, so as to stabilize the computations. Furthermore, clipping is done when $\nu_t < 0$, i.e., set $\nu_t = 0$ in such cases. When the eddy viscosity in Eq. (6) is computed from the above it is added to the molecular viscosity ν_0, calculated from the statement of the problem, to obtain the total viscosity ν, i.e., $\nu = \nu_0 + \nu_t$; ν can then be used to compute the "effective" relaxation times for hydrodynamic moments in the MRT-LBM (Sec. 2). Implementation of the dynamic SGS model in the MRT-LBM requires careful consideration of the following factors. First is the choice of the test-filter in the computation of the M_{ij} tensor. To conform naturally with the underlying cubic lattice grid structure, the discrete trapezoidal filter, which also allows for a simple dimension-wise implementation can be considered [51], as used in this work. Another issue is the implementation of the test-filters near grid interfaces in a multiblock approach, which requires careful use of averaging procedures, as discussed in Ref. [51]. Furthermore, optimization strategies should be fully considered for incorporating the dynamic procedure in the MRT-LBM to allow for an efficient implementation.

4 Multiblock Local Grid Refinement

The use of grids fine enough to resolve the wall regions, where the turbulence structures are smaller, throughout the domain can result in significant computational cost. This can be mitigated by introducing coarser grids farther from the wall, where turbulent length scales are generally larger. One approach is to consider using continuously varying grid resolutions, using an interpolation augmented formulation [56] that effectively decouples particle velocity space represented by the lattice and the computational grid. However, it is well known that interpolation could introduce significant numerical dissipation (see, e.g., Ref. [21]), which could severely affect the accuracy of solutions involving turbulent fluctuations. Thus, we consider locally embedded grid refinement approaches. In broad terms, there are two such versions—one in which the coarse and fine grids are adjacent [57,58] that use interpolations for inter-grid information transfer, and the other considers staggered grid arrangement [59,60]. As the latter version is conservative [59,60], it preserves mass and momentum conservation, and it is considered in this work.

Figure 2 shows a schematic of such a multiblock approach in which a fine cubic lattice grid is used close to the bottom wall surfaces and a coarser one, again cubic in shape, farther out. In

Downloaded From: https://fluidsengineering.asmedigitalcollection.asme.org on 06/30/2019 Terms of Use: http://www.asme.org/about-asme/terms-of-use

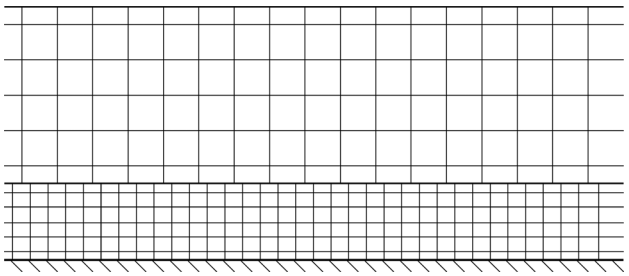

Fig. 2 Local grid refinement when using a staggered arrangement

order to facilitate the exchange of information at the interface between the grids, the spacing of the nodes changes by an integer factor, in this case two. As well as using different grid sizes, the two regions use different time steps (time step being proportional to grid size), and the computational cost required per unit volume is thus reduced by a factor of 16 in the coarse grid. Figure 2 shows a staggered grid arrangement, in which nodes on the fine and coarse sides of the interface are arranged in a manner that facilitates the imposition of mass and momentum conservation. Different blocks communicate with each other through the *Coalesce* and the *Explode* steps; in addition to the standard *stream-and-collide* procedure [59,60]. Essentially, the *Coalesce* procedure involves summing the particle populations on the fine nodes to provide new incoming particle populations for the corresponding coarse nodes. Similarly, the *Explode* step involves redistributing the populations on the coarse node to the surrounding fine nodes.

For completeness, we will now briefly discuss the key elements of the local grid refinement procedure. To illustrate the grid communicating steps, a magnified view of the nodes near the interface is shown in Fig. 3. Since there can be many different levels of grid refinement, the procedure may be best described by means of the following pseudocode involving recursion:

```
subroutine Loop(integer level)
  if(level < 0) return
  Loop(level-1)
  Loop(level-1)
  Advect(level)
  Boundaries(level)
  Coalesce(level)
  Collide(level)
  Explode(level)
  return
end
```

The `Loop` piece of code is a recursive subroutine which is initially called for the coarsest grid, and is then called for successively finer grids. The grids are assigned a property level such that the finest has `level=0`, the next finest `level=1`, and so on. The first step in this subroutine is to check whether all the grids have already been done; if not the Loop routine is called for the next finer levels. In the code above, this call is made twice, which is appropriate for the case where node separations change by a factor of two between successive grids. The number of calls is equal to the grid spacing ratio. The steps within this procedure are briefly described below.

`Advect(level)`

The streaming step-particle populations on the grids with the corresponding value of `level` propagate from one node to another.

`Boundaries(level)`

The boundary conditions are imposed on the grids of the current level

`Coalesce(level)`

This step involves communication between grids of different levels. For velocity directions in the boundary region pointing into the coarser grid, the particle populations on the fine nodes are summed to give new incoming particle populations for the coarse grid. In Fig. 3, this corresponds to summing the populations on the blue (small) nodes within the dotted square to give the population for the red (large) node. In terms of the density distribution function, this can be expressed as

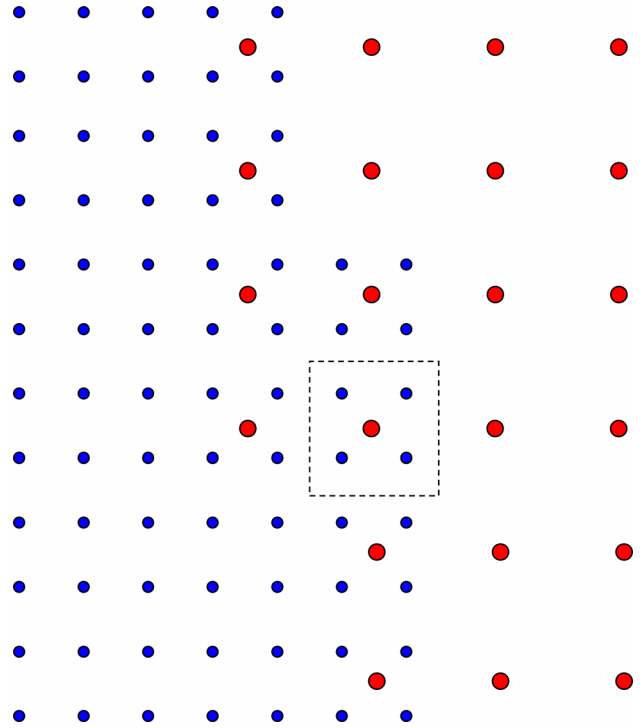

Fig. 3 Interface between coarse and fine grid when using a staggered arrangement

$$f_\alpha^c(\vec{x},t) = \frac{1}{r^D}\sum_{i=1}^{r^D} f_\alpha^f(\vec{x}_i,t) \tag{9}$$

where the superscripts c and f correspond to coarse and fine grid nodes, respectively, r is the grid refinement ratio (usually $r=2$) is the number of spatial dimensions ($D=3$ for three dimensional models), and the subscript i refers to adjacent fine grid nodes corresponding to a coarse grid node. Owing to the special staggered grid arrangement and the use of this coalesce step, conservation of mass and momentum is maintained.

`Collide(level)`

This routine performs the local collision step based on the MRT formulation for the grids of the current level. Note that collisions are not performed for nodes on the interface with a coarser grid; for example, the blue nodes lying inside the dotted square in Fig. 3.

`Explode(level)`

This is the other step dealing with exchange of information between grids of different levels. For velocity directions pointing into the fine grid, the particle populations on coarse grid nodes in `level` at the boundary are homogeneously redistributed to the fine grid nodes `level-1` according to:

$$f_\alpha^f(\vec{x},t) = f_\alpha^c(\vec{x}_i,t) \tag{10}$$

It may be noted that [60] does not explicitly apply rescaling as they suggest it to occur implicitly by the scheme itself in the specific volumetric grid arrangement employed. On the other hand, we considered an additional rescaling of the nonequilibrium part of the distributions (or, equivalently, the nonequilibrium moments corresponding to the viscous modes in the MRT framework, i.e., $\hat{f}^{neq,c} = (\Delta t_c/s_{\nu,c})(\Delta t_f/s_{\nu f})\hat{f}^{neq,f}$, where $s_\nu = 1/(3\nu/\Delta t + 1/2)$)

Downloaded From: https://fluidsengineering.asmedigitalcollection.asme.org on 06/30/2019 Terms of Use: http://www.asme.org/about-asme/terms-of-use

in our implementation similar to Ref. [61] after the streaming step at each grid level, though their effect on the results was found to be minor in the staggered grid formulation consistent with prior observations [60]. Such an approach has been validated in various prior studies for different applications (e.g., Refs. [51,62]). For a more recent related work involving rescaling and interpolations in the on-node MRT based grid refinement implementation, see Ref. [48]. We also plan to pursue such an alternative formulation in our future studies, while taking into account the near-wall physics involving the turbulence damping effects (as done here self-consistently using the dynamic procedure), which seem to have been neglected in Ref. [48].

5 Problem Specification

Let us now discuss the specific geometrical setup, computational conditions as well as the boundary conditions, particularly those at the inlet and outlet, considered for the turbulent flow over a backward facing step.

5.1 Geometrical Configuration and Computational Conditions. The geometry of the computational domain is illustrated schematically in Fig. 4. The total length and height of the domain are $32\,h$ and $6\,h$, respectively, with an extent in the spanwise direction of $4\,h$. Here h is the step height. The ratio of the heights downstream and upstream of the step, i.e., the expansion ratio is $ER = 1.2$. The Reynolds number Re_h based on the maximum free stream velocity U_0 and the step height is 5100. The boundary layer thickness at the step is about $1.2\,h$. This arrangement and the flow condition is the same as that reported in prior studies [5–7]. The origin of the coordinate system is taken to be at the lower step corner. The inlet is at the left boundary, $x = -12\,h$, and the mean inflow velocity profile was set to that obtained from Spalart's boundary layer DNS data [63]. Perturbations were carefully superimposed on this inflow mean velocity profile in order that the correct turbulence characteristics would develop in the approach to the step, as discussed below (see Sec. 5.2 for details). For the outlet, a convective boundary condition is employed (see Sec. 5.3). A zero-stress boundary was applied at the upper surface ($z = 6\,h$) and no slip condition at the walls was imposed using the half-way bounce back approach [64]. The domain was periodic in the spanwise (y) direction.

A note regarding the effect of the choice of relaxation times of the collision model on the location of the no-slip wall boundary condition is in order. A number of studies [26–29] have shown that at least two different relaxation times, when appropriately parameterized, are necessary to minimize the undesirable viscosity dependent discrete kinetic effect of locating wall boundaries. For example, for simulating a parabolic velocity profile corresponding to a laminar flow in a channel of actual height H, it can be shown that the following parametric relation results (e.g., Ref. [29]): $H^2 = H_{1/2}^2 + 4\Delta^2 - 1$. Here, $H_{1/2} = N\delta_x$, where N is the number of fluid nodes spanning across the channel, and $\Delta = (4/3)(1/s_\nu - 1/2)\left(1/s_q - 1/2\right)$, where s_ν and s_q are the relaxation parameters of the second-order (viscous) or even moments and the third-order or odd moments, respectively. To avoid the discrete kinetic effects, i.e., to ensure $H = H_{1/2}$, this means that $s_q = 8(2 - s_\nu)/(8 - s_\nu) = 16\nu/(8\nu + 1)$. The precise formulation of such parametric relations have been found to depend on the choice of the moments, the structure of the equilibria, as well as the type of flow [65]. On the other hand, if s_q is not set according to the above, or if only the SRT model with a relaxation parameter $1/\tau$ is employed, then the deviation from the actual boundary in the case of *steady* laminar flow is $\Delta = 4/3(\tau - 1/2)^2 = 12\nu^2$. For typical ranges of the relaxation parameter, it follows that the error of inaccurate boundary location lies within one lattice spacing. As Δ scales quadratically with the viscosity, the above considerations become important for slow or creeping flows with Reynolds number $\mathrm{Re} \ll 1$.

It should be carefully noted that the formula for the relaxation times mentioned above is based on the assumption of neglecting the unsteady term that arise in the emergent macroscopic equations [26,27], and hence is no longer "exact" for time-dependent flow problems, even within the laminar flow regime. This is particularly so for problems involving strongly unsteady features, i.e., consisting of high frequency flow components. As already noted in Ref. [27], further work is required to address these classes of problems within the laminar flow context. In the case of turbulent flow, an inherently time-dependent problem, one not only cannot neglect the role of unsteady emergent terms but also need to take into account other features due to its multiscale nature. Clearly, since the above formula based on steady laminar flow physics is not valid for turbulent flows, it is no wonder that the LB literature has invariably used bounce-back type schemes that do not involve adjustment of relaxation times for the latter problems (see, e.g., Ref. [48] for a recent study).

In any case, in particular, the additional factors involved for the LES of turbulent flows using the LBM are as follows. First, the Reynolds number is relatively very high $\mathrm{Re} \sim O(10^3) - O(10^5)$, and hence the molecular viscosity ν_o is relatively very small. Second, while the eddy viscosity ν_t in the relation $\nu = \nu_o + \nu_t$, where ν is the total viscosity, can vary significantly both spatially as well as temporally, near-wall turbulence physics dictates that they should rapidly tend towards zero as walls are approached. In fact, ν_t should satisfy the near-wall asymptotic scaling $\nu_t \sim O(z_+^3)$, where z_+ is the wall normal distance in viscous units (see, e.g., Refs. [50,66]). Thus, in the all-important near-wall region (say, $z_+ < 15$), much of the contribution for the total viscosity comes from the molecular viscosity ν_o, which is already relatively small given the chief interest is in the high Reynolds number turbulent flow. Most of the eddy viscosity; on the other hand, is generated due to shear *only* in the bulk region away from the walls. In other

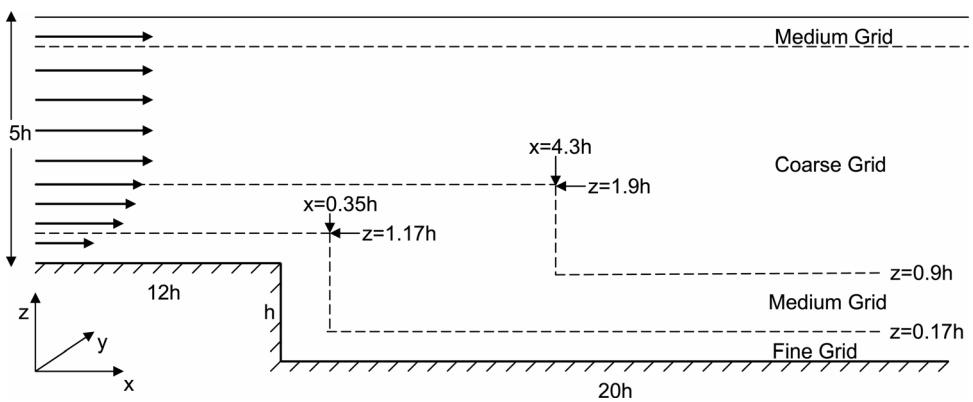

Fig. 4 Schematic representation of geometry. Step is at *x/h* = 0 and *z* = 0 corresponds to lower boundary. Note that dimensions of some regions are exaggerated to ensure clarity.

Downloaded From: https://fluidsengineering.asmedigitalcollection.asme.org on 06/30/2019 Terms of Use: http://www.asme.org/about-asme/terms-of-use

words, given that $\nu \approx \nu_o \ll 1$ is in the near-wall region, the deviation Δ from the actual location, while within one lattice spacing δ_x nevertheless becomes relatively small. Third, and finally, by being a multiscale problem, near-wall turbulence physics requires that the lattice spacing in the vicinity of the walls be generally kept relatively small, of the order of the Kolmogorov scale, akin to that used in DNS (while the bulk region scales may be much larger). These various aspects fortunately make the issue of the deviation Δ involved in locating the boundary relatively much less prominent for LES of turbulent flow, when compared to that for problems such as Stokes flows. Since $\nu \approx \nu_o \ll 1$ in the near-wall regions, the issue of numerical stability becomes a significant concern for high Re turbulent flow LES. In such situations, in our experience, the SRT-LBM was found to become unstable for a given choice of resolution, while the MRT-LBM is able to provide robust simulations by carefully separating various relaxation times for the kinetic modes. Also of interest to note here is that Ref. [29] found that maintaining a parametric relation between the relaxation parameters to minimize viscosity related discrete effects such as that presented above tends to make the approach less stable. As seen from the results of our prior studies and the current work, the use of interpolated bounce back condition for LES of turbulent flows was found to give satisfactory results. Nevertheless, for the purpose of generality and rigor, it would be interesting to derive the parametric relation between the relaxation times with *variable* viscosity (which satisfies a specified variation) for turbulent flows with a given *mean* velocity profile (e.g., $1/7^{th}$ power law), following the analytical approach presented in Ref. [27]. Such studies may also take special significance for RANS, where the near-wall effects are implicitly modeled by means of a slip velocity using a log-law, i.e., using a wall function approach (this can be extended to other types of problems as well, including non-Newtonian variable viscosity flows). These are subjects for future investigations.

Let us now discuss the grid resolution employed for simulating the turbulent flow over a backward facing step. As shown in Fig. 4, three different grid resolutions were employed in a multiblock approach. The finest grid had a size, $\Delta = \delta_x$ such that the step size is resolved by 64 grid nodes ($h = 64\delta_x$); the medium grid was twice the size of the fine grid and the spacing of the coarse grid was twice that of the medium grid. The nodes nearest to the wall were spaced two wall units from the wall ($\Delta^+ = 2$). This was found to be adequate to fairly resolve the near-wall turbulence structures in prior studies [25,51]. While the use of the bounce back boundary condition does not necessarily maintain the location of the wall exactly half-way between the two adjacent nodes, for the simulation of turbulent flow, the deviation from the actual location turns out to be relatively small. This can be numerically demonstrated based on analytical considerations of the mean velocity profile in the universal viscous sublayer region carried out for a well-defined wall-bounded turbulent flow. Appendix B presents such a calculation and shows that it is practically adequate to use such a boundary condition for a turbulent flow simulation. The eddy viscosity has negligible contribution in the entire viscous sublayer, with about three to four orders of magnitude smaller than the molecular viscosity. Furthermore, the latter is also relatively very small in a turbulent flow resulting in overall minor deviation in wall location, confirming our earlier arguments. Further refinement in accuracy could, in principle, be possible by constructing and using new expressions for the relaxation times for the third-order moments based on considerations of the mean velocity profile derived from turbulence physics. In any case, from the above it follows that the finest grids had a resolution of about four wall units, with the medium and coarse grids 8 and 16, respectively. To reduce the computational cost while maintaining the necessary free stream flow physics, a medium grid with a thickness of $0.25\,h$ is employed in the vicinity of the zero-stress upper boundary. As discussed in Sec. 4, the multiblock grids were arranged in a staggered manner to satisfy conservation of hydrodynamic fields.

Of course, based on our current state of knowledge, it is impossible to precisely locate the boundary using bounce-back type formulations in LB algorithms, regardless of how the sets of relaxation parameters are tuned, for *turbulence* simulation. The specific parametric relation between two relaxation parameters was developed to strictly work for steady laminar flows [26,27]. Due to the lack of a proper alternative, we have used the bounce-back scheme without tuning relaxation parameters in this regard in the present work. This is similar to various LES-LBM studies existing in the literature (for recent work, see, e.g., Ref. [48]). However, as discussed above, this does not necessarily imply a significant limitation in the context of turbulent flows. Here, it should be noted that numerical schemes used for LES, be it based on LBM or NS-based solvers, and experimental techniques for turbulence are generally associated with various sources of uncertainty errors. For example, even in the NS-based LES that are devoid of the issue mentioned above, there are various numerical aspects that introduce uncertainties in the results (see, e.g., Ref. [67] for a detailed discussion). It is only meaningful to make proper comparison in a statistical sense for turbulent flows between the simulation results and prior data and the adequacy is established if the former is within the uncertain error bounds. A recent LES-LBM study mentioned above [48] has shown good agreement for various turbulence statistics, stresses, coefficients of pressure and drag for flow past a sphere. This is consistent with our earlier discussion related to the boundary conditions in turbulent simulations using the LBM. Similarly, in the present work, we will see a good agreement between our simulation results and the prior data (involving measurement data and DNS), of course within their uncertainty error ranges, when detailed comparisons are made for the statistics involving velocity field, components of Reynolds stresses and the spatial development of the coefficient of pressure along the backward facing step.

The following note is in order regarding the estimated computational efficiency achieved with the use of the multiblock grid strategy in place of the uniform grid implementation throughout the domain. Overall, the collision step executed via the MRT formulation, whose computational cost is similar to the standard implementations, comprises the main computational element for a given grid level; the streaming step is just the regular memory shift operation and the inter-grid transfers comprise a minor overhead. In general, as discussed earlier, the medium grid reduces the computational cost by a factor of 16 when compared to the fine grid, since both the space step and the time step are increased in the same proportion. Similar cost reduction factor exists between the coarse grid and the medium grid. Now, the total volume of the computational domain shown in Fig. 4 in terms of the step height h is $720h^3$. For the particular multiblock gridding approach employed, the fine, medium and coarse grids occupy the volumes of $23.2h^3$, $141.2h^3$ and $555.6h^3$, respectively. This yields a factor of $72/(23.2 + 141.2/16 + 555.6/256)$ or about 21 reduction in the computational cost when the multiblock grid approach is used in lieu of the single uniform fine grid throughout the domain.

5.2 Inflow Conditions. Unlike in RANS, for LES one must carefully provide information on the time-dependent characteristics of the eddy motion, i.e., the fluctuating component of velocity, at the inlet. The overall velocity at the inlet can then be expressed as

$$u(y,z,t) = \langle u(z) \rangle + u'(y,z,t) \tag{11}$$

where $\langle u(z) \rangle$ is the mean, or ensemble averaged, velocity, and is $u'(y,z,t)$ is the corresponding fluctuating component. For the mean velocity profile, possible choices based on semiempirical considerations include an approximate one seventh power law or a Blasius profile. Alternatively, it can be taken from experimental or, as was done here, DNS data for the boundary layer flow [63].

The specification of the fluctuating component u' (dependent on spanwise coordinate y and time t as well) that preserves the

Downloaded From: https://fluidsengineering.asmedigitalcollection.asme.org on 06/30/2019 Terms of Use: http://www.asme.org/about-asme/terms-of-use

essential features of inflow turbulence characteristics (such as the Reynolds stress) presents a significant challenge. Ideally one might hope to use the output from a DNS of a turbulent boundary layer to provide the inlet conditions. In practice, the data will not, in general, be available for specific situations, and other techniques have been developed to generate suitable inflow turbulence conditions [3]. One of the simplest approaches is to impose a white noise with length and time scales equal to the grid spacing and time step, i.e., random velocity at the inlet plane. This rudimentary method has a number of limitations—it yields few low frequency/low wavenumber fluctuations while providing an excess of high frequency perturbations. As a result, it is found that this artificial turbulence rapidly dissipates downstream from the inlet. A more realistic approach is based on the information from the energy spectrum [68,69]. Here, the fluctuating turbulent field is expressed as a Fourier series, whose amplitudes are chosen to be consistent with the energy spectrum and phases to produce the correct Reynolds stress. It requires considerable distance from the inlet for the development of the required turbulent velocity field incurring significant computational expense [70]. Alternatively, a recycling approach [71], in which an additional computational domain is placed upstream of the main domain, can be employed. The conditions at the end of this section are used for the inlet conditions both for the main domain and for this section. In practice, for a spatially developing flow, such as a boundary layer, it is also necessary to perform some rescaling when transferring the field from the downstream boundary to the upstream boundary. It may be noted that by applying carefully designed body force at a number of planes downstream of the inlet promotes the development of desired Reynolds stress profile with these methods [72].

In this work, we have employed the reconstruction procedure [73], which is simpler and computationally more efficient. The key idea behind this method is to reconstruct the typical turbulence structures by imposing several disturbances with different characteristics which correspond in frequency and wavelength to typical scales found in the flow being modeled. It is a modification of an earlier proposed approach [74]. Specifically, it considers four modes, one in the inner layer that represents the effect of near-wall streaks, and three or more further modes that perturb at different levels in the outer flow. The velocity perturbations at the inlet is given by [73]

$$u'_k(y,z,t) = u_* \sum_{j=1}^{N} C_{kj} \cos(\beta_j y + \phi_j) \sin(2\pi t^*/\tau_j) f(z, z_j^{\max}) \quad (12)$$

where the index k denotes the Cartesian velocity component, j the mode with $N=4$ and u_* is the friction velocity. The values of various constants in Eq. (12) are given in Table 1. The envelope function $f(z, z_j^{\max})$ is written as

$$f(z, z_j^{\max}) = \left[\left(\frac{z}{z_j^{\max}} \right)^n \exp\left(-\left(\frac{z}{z_j^{\max}} \right) \right)^n \right]^m \quad (13)$$

in which $m=2$ for $k=3$ and $j>1$, and unity otherwise. The parameter n is given by $n = 1-(1+\tanh(10(z-z^{\max})))/6$ for the first mode, i.e., $j=1$, and is unity otherwise. In Table 1, t_d is the displacement thickness. Note that only the streamwise ($k=1$) and wall-normal ($k=3$) components are calculated from above. The spanwise component is computed so as to satisfy divergence free condition of the perturbed velocity field.

Table 1 Parameters for inflow turbulence

j	C_{1j}	C_{3j}	τ_j	β_j	ϕ_j	$z_j^{\max}$
1	15.2	−7	100	$2\pi/100$	0	12
2	5.6	−2.8	32	$2\pi/133$	0.1	t_d
3	5.6	−2.8	58	$2\pi/200$	0.2	$2t_d$
4	5.6	−2.8	109	$2\pi/400$	0.3	$3t_d$

To assess this approach, a series of numerical experiments were conducted in which a boundary layer was simulated by using the inlet mean velocity profile based on the DNS data and superimposing a perturbation using Eq. (12) as inlet conditions. Turbulence statistics were collected at locations several boundary layer thickness downstream of the inlet and compared with DNS data [63]. Different parameters were varied, and the set found to give the best performance is shown in Table 1, and a value of 49 wall units was used for the displacement thickness t_d. In addition, a small amount of random noise was added to the inlet velocities, and no perturbation was applied for $z^+ > 250$. These considerations preserved the mean velocity and turbulent fluctuations in the boundary layer development downstream of the inlet for simulation of flow past the step.

5.3 Outflow Boundary Conditions. At the outlet, a convective condition was used, which can be specified as

$$\frac{\partial u}{\partial t} + U_c \frac{\partial u}{\partial x} = 0 \quad (14)$$

where U_c is a convective velocity, typically set to the free stream velocity. This choice for the boundary causes the unsteady turbulence structures to propagate out of the domain. Furthermore, it tends to maintain numerical stability of the overall approach.

6 Results and Discussion

In order to let the flow establish a statistically stationary state, the simulation was initially run for a period of $300h/U_0$, where U_0 is the maximum free stream velocity. Such a large startup period is necessary as fluid elements have large residence time in the recirculation region [6]. The computation was continued for a further duration of $200h/U_0$ during which various statistics of the flow field were collected. Parallel processing strategy was employed by running the computation using 16 processors. Mean flow velocity profiles and turbulence statistics were compiled from fully three-dimensional turbulent field by averaging over both time and the homogeneous spanwise direction. Comparisons of the computed structure of the development of the turbulent flow field were made with the DNS data [6], experimental data [7], as well as prior LES results [5].

Figure 5 shows a comparison of the computed velocity profiles with the DNS data [6] at different selected stations in the recirculation, reattachment and recovery regions. The dramatic changes in the velocity profiles of these regions is well reproduced by the multiblock MRT-LBM using the dynamic SGS model, and is in excellent agreement with DNS. In particular, as noted in Ref. [6], the velocity profile is yet to reach a fully developed equilibrium boundary layer profile at the farthest location considered, i.e., $x/h=19$, where it exhibits an inflection point. This is consistent with the observation that for the relatively low Reynolds number

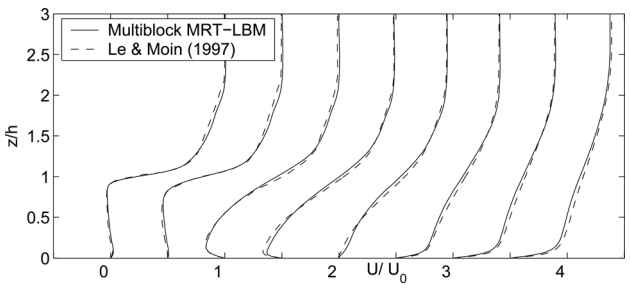

Fig. 5 Mean streamwise velocity profiles. From left to right, positions are $x/h = 0.5, 1, 2.5, 4, 6, 10, 15, 19$; successive profiles are offset by U_0 on abscissa: (–) this study; (- -) DNS [6].

Downloaded From: https://fluidsengineering.asmedigitalcollection.asme.org on 06/30/2019 Terms of Use: http://www.asme.org/about-asme/terms-of-use

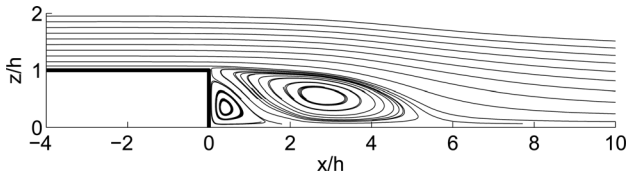

Fig. 6 Mean streamlines computed by the multiblock MRT-LBM using the dynamic SGS model. Note that vertical coordinate is exaggerated by a factor of two for clarity.

considered, as the flow experiences sudden expansion over the step, it is subject to an appreciable adverse pressure gradient in the streamwise direction that prevents maintenance of the equilibrium boundary layer, i.e., the asymptotic logarithmic law.

The complex flow structure involving flow separation and reattachment can more clearly be observed by means of the mean streamlines obtained by LES, which is shown in Fig. 6. In addition to the main recirculation bubble, a relatively large secondary bubble can also be seen in the step corner, consistent with DNS [6]. An important quantitative measure characteristic to the recirculation region is the reattachment length X_r. There are a few different methods in which the location of the reattachment point can be determined all of which give almost identical results for this problem [6]. The approach used here was to find the location at which the mean velocity changes sign, which gave a value of $X_r = 6.0$ for the location of the reattachment point. This compares well with the value of 6.1 obtained in the LES reported by Akselvoll and Moin (1993) [5], who also noted a value of 6.0 with their prior fine grid calculation, i.e., DNS; the more recent DNS of Le et al. (1997) [6] obtained a value of 6.28. The corresponding measurements in the experiments by Jovic and Driver (1994) [7] found the value of X_r to vary between 6.0 and 6.1. Plots of the computed instantaneous spanwise vorticity are shown in Fig. 7. It can be observed that the free shear layer region leads to flow separation, as seen by a quiescent region in the lee of the step; subsequently,

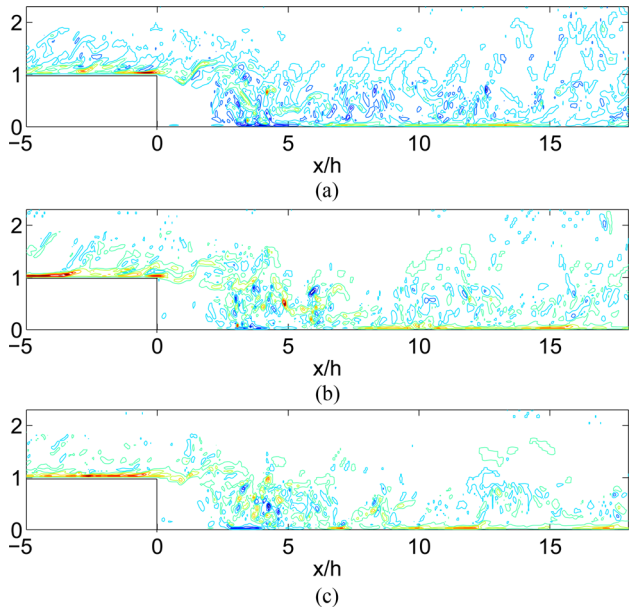

Fig. 7 Instantaneous values of the vorticity computed by the multiblock MRT-LBM using the dynamic SGS model for three different representative times

the region of high vorticity spreads out towards the bottom wall in the recovery region.

An important measure of the turbulent activity in the flow field is provided by the second-order turbulent statistics. Figure 8 presents a comparison of the structure of turbulence statistics at a number of locations downstream of the step. Generally, good agreement is seen for various components of turbulent intensities and Reynolds stress, demonstrating the ability of the multiblock MRT-LBM using the dynamic SGS model to reproduce complex

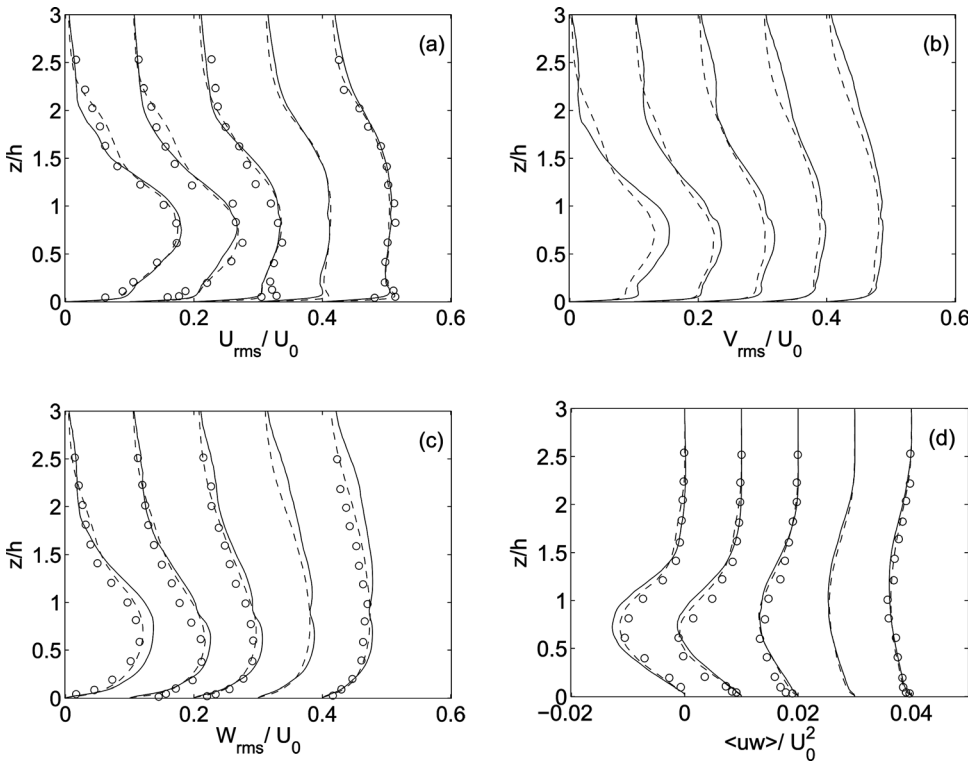

Fig. 8 Turbulence intensities and Reynolds stress downstream of the step at different stations: (–) multiblock MRT-LBM using the dynamic SGS model; (- -) DNS [6]; (o) experiment [7]

Downloaded From: https://fluidsengineering.asmedigitalcollection.asme.org on 06/30/2019 Terms of Use: http://www.asme.org/about-asme/terms-of-use

turbulence physics. The influence of the SGS model, in comparison with just performing a coarse DNS, is now demonstrated. In this regard, an earlier study by Akselvoll and Moin (1993) [5] provides both coarse and fine DNS data, along with LES results using the dynamic SGS model based on the solution of the NS equations for turbulent statistics close to the corner in the recirculation region at $x/h = 2$, which is used for comparison in Fig. 9. Evidently, the LES results of the turbulent intensities and the Reynolds stress using the dynamic SGS model, based on both the NS [5] and the multiblock MRT-LBM (this study) is in much better agreement with the fine DNS than the corresponding coarse DNS calculations. Thus, the use of a subgrid scale model is necessary to correctly reproduce the resolved turbulent stresses, as the coarse grid computations without a model is unable to do so, substantially overpredicting them. In future work, it would be interesting to study the effects of different SGS models.

Finally, we report the variation of the step-wall pressure in terms of the nondimensional pressure coefficient C_p defined by

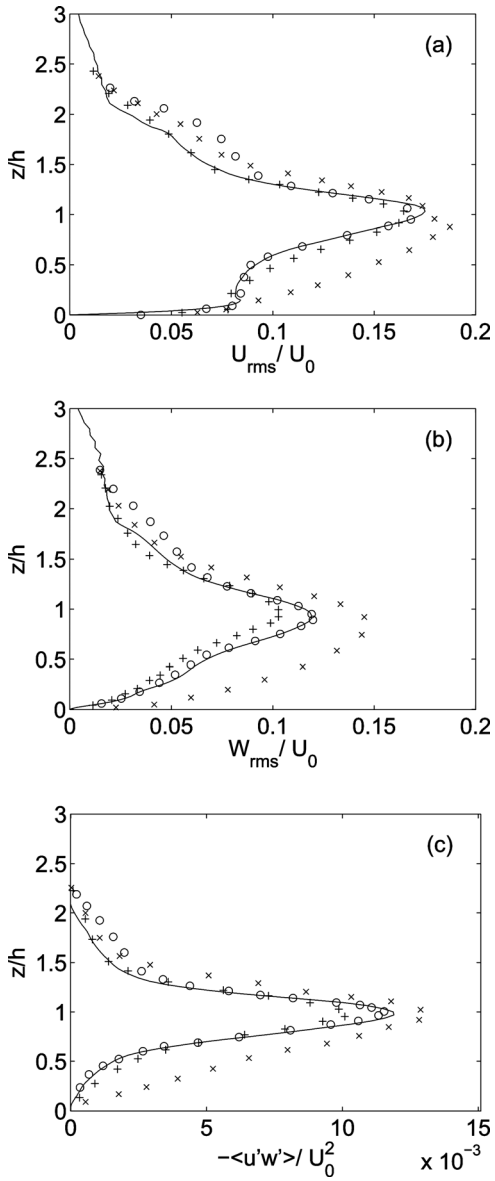

Fig. 9 Comparison of turbulence intensities and Reynolds stress close to the corner in the recirculation region at $x/h = 2$: (–) multiblock MRT-LBM using the dynamic SGS model; (o) DNS [5]; (+) LES [5]; (×) coarse DNS [5]

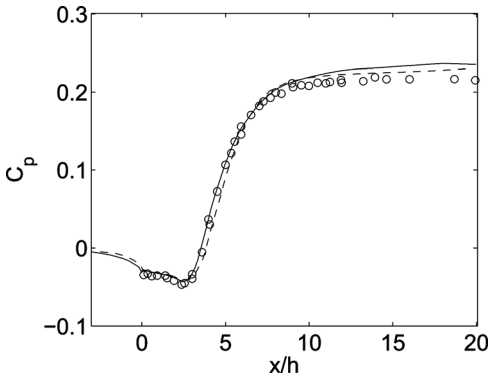

Fig. 10 Comparison of the variation of the step-wall pressure coefficient: (–) multiblock MRT-LBM using the dynamic SGS model; (- -) DNS [6]; (o) experiment [7]

$$C_p = \frac{2(P - P_0)}{\rho U_0^2} \tag{15}$$

where P_0 is the reference pressure measured at $x/h = -5$, for comparison with prior data. Figure 10 shows the variation of C_p as a function of the streamwise distance x/h, where a comparison with the DNS [6] and experimental [7] data is also made. The structure of the strong adverse pressure gradient in the downstream of the step, particularly in the reattachment region, is evident. While just like in DNS, some difference between the computed results and experimental data is observed in the recovery region, overall, the LES results are in very good agreement with the DNS.

7 Summary and Conclusions

In this paper, we discussed the computation of a complex external turbulent flow over a backward facing step using the lattice Boltzmann method. Large eddy simulations were performed by incorporating a dynamic procedure for the Smagorinsky SGS model in a multiple relaxation time formulation using multiblock grids to achieve accurate and efficient implementation. Flow boundary conditions were introduced carefully to correctly maintain the essential features of turbulence by using a reconstruction procedure at the inlet and a convective boundary condition at the outlet. Parallel computations were performed to obtain the turbulence statistics for a Reynolds number based on the step height and maximum free stream velocity of 5100 and an expansion ratio of 5.1. It was found that the mean velocity profile is in excellent agreement with DNS throughout the entire domain, including the recirculation, reattachment and recovery regions. The reattachment length was found to be 6.0 times the step height, which agrees very well with prior DNS and experimental data, as well as LES based on Navier–Stokes equations. Furthermore, the structure of turbulence intensities and Reynolds stress and the pressure distribution obtained using the multiblock MRT-LBM with a dynamic SGS model were in good quantitative agreement with prior data.

Acknowledgment

This work was performed under the auspices of the National Aeronautics and Space Administration (NASA) under Contract No. NNL07AA04C. Computational resources were provided by the Office of Science of DOE under Contract DE-AC03-76SF00098 and the City College New York, CUNY.

Appendix A: Components of the Moments Their Equilibria and Strain Rate Tensor for D3Q19 Model

The components of the various elements in the moments are as follows [22]:

Downloaded From: https://fluidsengineering.asmedigitalcollection.asme.org on 06/30/2019 Terms of Use: http://www.asme.org/about-asme/terms-of-use

$$\hat{f}_0 = \rho, \quad \hat{f}_1 = e, \quad \hat{f}_2 = e^2, \quad \hat{f}_3 = j_x, \quad \hat{f}_4 = q_x, \quad \hat{f}_5 = j_y,$$
$$\hat{f}_6 = q_y, \quad \hat{f}_7 = j_z, \quad \hat{f}_8 = q_z, \quad \hat{f}_9 = 3p_{xx}, \quad \hat{f}_{10} = 3\pi_{xx},$$
$$\hat{f}_{11} = p_{ww}, \quad \hat{f}_{12} = \pi_{ww}, \quad \hat{f}_{13} = p_{xy}, \quad \hat{f}_{14} = p_{yz}, \quad \hat{f}_{15} = p_{xz},$$
$$\hat{f}_{16} = m_x, \quad \hat{f}_{17} = m_y, \quad \hat{f}_{18} = m_z$$

Here, ρ is the density, e and e^2 represent kinetic energy that is independent of density and square of energy, respectively; j_x, j_y, and j_z are the components of the momentum, i.e., $j_x = \rho u_x$, $j_y = \rho u_y$, $j_z = \rho u_z$, q_x, q_y, q_z are the components of the energy flux, and p_{xx}, p_{xy}, p_{yz}, and p_{xz} are the components of the symmetric traceless viscous stress tensor; The other two normal components of the viscous stress tensor, p_{yy} and p_{zz}, can be constructed from p_{xx} and p_{ww}, where $p_{ww} = p_{yy} - p_{zz}$. Other moments include: π_{xx}, π_{ww}, m_x, m_y, and m_z. The first two of these moments have the same symmetry as the diagonal part of the traceless viscous tensor p_{ij}, while the last three vectors are parts of a third rank tensor, with the symmetry of $j_k p_{mn}$. The corresponding components of the equilibrium moments, which are functions of conserved moments, i.e., density ρ and momentum $\vec{j}$, are as follows [22]:

$$\hat{f}_0^{eq} = \rho, \quad \hat{f}_1^{eq} \equiv e^{eq} = -11\rho + 19\frac{\vec{j}\cdot\vec{j}}{\rho},$$
$$\hat{f}_2^{eq} \equiv e^{2,eq} = 3\rho - \frac{11}{2}\frac{\vec{j}\cdot\vec{j}}{\rho}, \quad \hat{f}_3^{eq} = j_x, \quad \hat{f}_4^{eq} \equiv q_x^{eq} = -\frac{2}{3}j_x,$$
$$\hat{f}_5^{eq} = j_y, \quad \hat{f}_6^{eq} \equiv q_y^{eq} = -\frac{2}{3}j_y, \quad \hat{f}_7^{eq} = j_z, \quad \hat{f}_8^{eq} \equiv q_z^{eq} = -\frac{2}{3}j_z,$$
$$\hat{f}_9^{eq} \equiv 3p_{xx}^{eq} = \frac{\left[3j_x^2 - \vec{j}\cdot\vec{j}\right]}{\rho}, \quad \hat{f}_{10}^{eq} \equiv 3\pi_{xx}^{eq} = 3\left(-\frac{1}{2}p_{xx}^{eq}\right),$$
$$\hat{f}_{11}^{eq} \equiv p_{ww}^{eq} = \frac{\left[j_y^2 - j_z^2\right]}{\rho}, \quad \hat{f}_{12}^{eq} \equiv \pi_{ww}^{eq} = -\frac{1}{2}p_{ww}^{eq},$$
$$\hat{f}_{13}^{eq} \equiv p_{xy}^{eq} = \frac{j_x j_y}{\rho}, \quad \hat{f}_{14}^{eq} \equiv p_{yz}^{eq} = \frac{j_y j_z}{\rho}, \quad \hat{f}_{15}^{eq} \equiv p_{xz}^{eq} = \frac{j_x j_z}{\rho},$$
$$\hat{f}_{16}^{eq} = 0, \quad \hat{f}_{17}^{eq} = p_{ww}^{eq} = \frac{\left[j_y^2 - j_z^2\right]}{\rho}, \quad \hat{f}_{12}^{eq} \equiv \pi_{ww}^{eq} = -\frac{1}{2}p_{ww}^{eq},$$
$$\hat{f}_{13}^{eq} \equiv p_{xy}^{eq} = \frac{j_x j_y}{\rho}, \quad \hat{f}_{14}^{eq} \equiv p_{yz}^{eq} = \frac{j_y j_z}{\rho}, \quad \hat{f}_{15}^{eq} \equiv p_{xz}^{eq} = \frac{j_x j_z}{\rho},$$
$$\hat{f}_{16}^{eq} = 0, \quad \hat{f}_{17}^{eq} = 0, \quad \hat{f}_{18}^{eq} = 0$$

For problems involving external forces $\vec{F}$, the components of the source terms in moment space can be found in Ref. [25].

The components of the strain rate tensor used in subgrid scale (SGS) turbulence model at the grid-filter level can be written explicitly in terms of nonequilibrium moments [44]

$$S_{xx} \approx -\frac{1}{38\rho}\left[s_1\hat{h}_1^{(neq)} + 19s_9\hat{h}_9^{(neq)}\right] \tag{A1}$$

$$S_{yy} \approx -\frac{1}{76\rho}\left[2s_1\hat{h}_1^{(neq)} - 19\left(s_9\hat{h}_9^{(neq)} - 3s_{11}\hat{h}_{11}^{(neq)}\right)\right] \tag{A2}$$

$$S_{zz} \approx -\frac{1}{76\rho}\left[2s_1\hat{h}_1^{(neq)} - 19\left(s_9\hat{h}_9^{(neq)} + 3s_{11}\hat{h}_{11}^{(neq)}\right)\right] \tag{A3}$$

$$S_{xy} \approx -\frac{3}{2\rho}s_{13}\hat{h}_{13}^{(neq)} \tag{A4}$$

$$S_{yz} \approx -\frac{3}{2\rho}s_{14}\hat{h}_{14}^{(neq)} \tag{A5}$$

$$S_{xz} \approx -\frac{3}{2\rho}s_{15}\hat{h}_{15}^{(neq)} \tag{A6}$$

where

$$\hat{h}_\alpha^{(neq)} = \hat{f}_\alpha - \hat{f}_\alpha^{eq}, \quad \alpha \in \{1, 9, 11, 13, 14, 15\} \tag{A7}$$

Here, $\hat{f}_\alpha$ and $\hat{f}_\alpha^{eq}$ are components of moments and their local equilibria. s_α are elements of the collision matrix $\hat{\Lambda} = \mathrm{diag}(s_0, s_1, \ldots, s_{18})$ in moment space. A generalization of the above expressions for the strain rate tensor in the presence of external forces is presented in Ref. [25].

Appendix B: Estimation of the Deviation in the Wall Location in a Turbulence Simulation Using the LBM

In order to quantitatively estimate any deviation in the wall location from that specified by means of the half-way bounce back scheme for turbulent flow simulation, we consider the following well-defined problem involving fully developed channel flow. We consider turbulent flow driven by a body force $F_x = 1.2437 \times 10^{-6}$ with the channel width resolved by $N = 45$ nodes in the wall normal direction (see Refs. [25,51,75] for details on the problem setup). The use of the half-way bounce back boundary condition implies that the specified channel width is $H_{1/2} = N \cdot \delta_x = 45$. The fluid viscosity and density are set to be $\nu_0 = 0.001833$ and $\rho_0 = 1.0$, respectively. The shear Reynolds number, which is based on the shear or friction velocity u_* typical for wall-bounded turbulent flows, is equal to 183.7. This corresponds to a nominal Reynolds number Re based on maximum velocity of 3485, and in the same order of magnitude for the flow past the backward facing step considered in this work. The simulation is carried out using the WALE SGS model [76], whose behavior in the near-wall region is similar to the general dynamic SGS model discussed in this work. In particular, both these models recover the physically correct near-wall asymptotic scaling for the decay of the eddy viscosity $\nu_t \sim O((z^+)^3)$.

Figure 11 shows the mean velocity profile as a function of the wall normal distance normalized by viscous scales (denoted by "+") in semilog coordinates, providing, in particular, a magnified view of its near-wall variation. Here, the mean velocity $\langle u \rangle$ is normalized by the friction velocity u_* (which is related to the driving force, see Ref. [25]) and the distance z by the viscous scale $\delta_\nu = \nu_0/u_*$, i.e., $z^+ = z/\delta_\nu$. In the *viscous sublayer region* ($z^+ \leq 5$) that adjoins the wall and below the log-law region, flow physics considerations yield the following analytical solution for the *mean* velocity profile (see, e.g., Ref. [66]):

$$\frac{\langle u \rangle}{u_*} = \frac{z}{\delta_\nu}, \quad \text{if} \quad \frac{z}{\delta_\nu} \leq 5 \tag{B1}$$

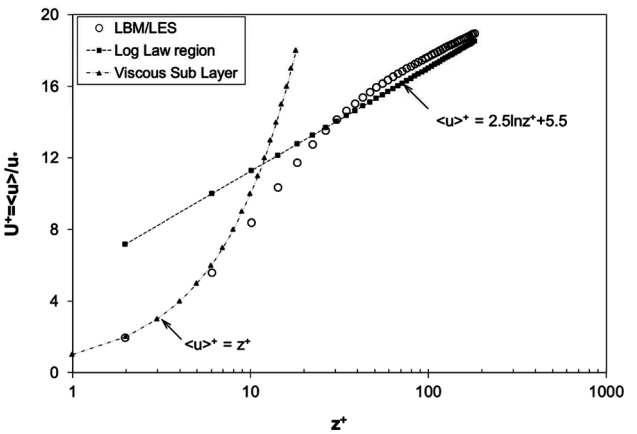

Fig. 11 Mean velocity profile in a fully developed turbulent channel flow at a shear Reynolds number $\mathrm{Re}_* = 183.7$ plotted as a function of the wall normal distance normalized by viscous scales in semilog coordinates

Downloaded From: https://fluidsengineering.asmedigitalcollection.asme.org on 06/30/2019 Terms of Use: http://www.asme.org/about-asme/terms-of-use

In our recent study for the same physical problem [75], we have found that in this viscous sublayer region, the eddy viscosity ν_t rapidly reduces from $\sim 10^{-5}$ to 10^{-6} (see Fig. 7 in Ref. [75]), and that the ratio of the eddy viscosity and the molecular viscosity ν_t/ν_0 correspondingly varies from 5.4×10^{-3} to 5.4×10^{-4}, respectively. Thus, the eddy viscosity ν_t is three to four orders of magnitude smaller than the molecular viscosity ν_0, with the former, as it should, having practically negligible contribution on the dynamics of flow in the viscous sublayer region. This is consistent with the well-known observation that almost entire momentum transfer in the viscous sublayer is due to the molecular mechanism, with the eddy transport having negligible contribution—a universal behavior of bounded turbulent flows (see also Fig. 7.4 in Ref. [66]).

Now, setting H to be the actual channel width observed in the turbulent flow simulation, and ε to be the deviation from the wall location prescribed by the half-way bounce back boundary condition on each side, we have $H = H_{1/2} + 2\varepsilon$. The friction velocity u_* mentioned above can be estimated from a global force balance, i.e., $F_x = \rho_0 u_*^2/H$ [51] yielding $u_*^2 = F_x(H_{1/2} + 2\varepsilon)/\rho_0$. Hence, using this and the expression for the viscous length scale δ_ν specified earlier, Eq. (B1) can be rewritten as $\langle u \rangle = z u_*^2/\nu_0 = z F_x(H_{1/2} + 2\varepsilon)/(\rho_0 \nu_0)$. Denoting z_1 to be the actual nearest or the first fluid node from the wall, we have $z_1 = 1/2 + \varepsilon$, at which we represent the mean velocity by $\langle u_1 \rangle$. Hence, the above considerations yield the following analytical expression for the mean velocity at the nearest fluid node:

$$\langle u_1 \rangle = \left(\frac{1}{2} + \varepsilon\right) F_x \frac{(H_{1/2} + 2\varepsilon)}{(\rho_0 \nu_0)} \tag{B2}$$

When the simulation is statistically converged, we obtain the value of the mean velocity field at z_1 as $\langle u_1 \rangle = 0.0146683$. Matching this value with the analytical solution given above should allow us in deducing the actual location of the wall boundary. Hence, substituting for the values of $\langle u_1 \rangle$, F_x, $H_{1/2}, \nu_0$, and ρ_0 leads to a quadratic equation in terms of the unknown ε, i.e.,

$$2\varepsilon^2 + (1 + H_{1/2})\varepsilon + \left(\frac{1}{2} H_{1/2} - \frac{\langle u_1 \rangle \rho_0 \nu_0}{F_x}\right) = 0 \tag{B3}$$

whose solution yields $\varepsilon = 0.019$ or the deviation in the wall location is less than 2% of the lattice mesh size. Thus, while in principle, the deviation ε is not exactly zero, in reality it is indeed relatively very small compared to the mesh spacing and hence the choice of the boundary condition is adequate for the simulation of turbulent flow.

References

[1] Armaly, B., Durst, F., Pereira, J. C. F., and Schonung, B., 1983, "Experimental and Theoretical Investigation of a Backward-Facing Step," J. Fluid Mech., **127**, pp. 473–496.

[2] Kaiktsis, L., Karniadakis, G. E., and Orszag, S. A., 1991, "Onset of Three-Dimensionality, Equilibria, and Early Transition in Flow Over a Backward-Facing Step," J. Fluid Mech., **231**, pp. 501–528.

[3] Sagaut, P., 1998, *Large Eddy Simulation for Incompressible Flows*, Springer, Berlin.

[4] Friedrich, R., and Arnal, M., 1990, "Analysing Turbulent Backward-Facing Step Flow With the Lowpass-Filtered Navier–Stokes Equations," J. Wind Eng. Ind. Aerodyn., **35**, pp. 101–128.

[5] Akselvoll, K., and Moin, P., 1993, "Large Eddy Simulation of a Backward Facing Step Flow," *Engineering Turbulence Modelling and Experiments 2*, W. Rodi, and F. Martelli, eds., Elsevier, Amsterdam, The Netherlands, pp. 289–309.

[6] Le, H., Moin, P., and Kim, J., 1997, "Direct Numerical Simulation of Flow Over a Backward-Facing Step," J. Fluid Mech., **330**, pp. 349–374.

[7] Jovic, S., and Driver, D. M., 1994, "Backward-Facing Step Measurement at Low Reynolds Number, $\mathrm{Re}_h = 5000$," NASA Technical Memorandum 108807, Washington, DC.

[8] Jovic, S., and Driver, D. M., 1995, "Reynolds Number Effects on the Skin Friction in Separated Flows Behind a Backward Facing Step," Exp. Fluids, **18**, pp. 464–467.

[9] McNamara, G. R., and Zanetti, G., 1988, "Use of the Boltzmann Equation to Simulate Lattice-Gas Automata," Phys. Rev. Lett., **61**, pp. 2332–2335.

[10] He, X., and Luo, L.-S., 1997, "A Priori Derivation of the Lattice Boltzmann Equation," Phys. Rev. E, **55**, pp. R6333–R6336.

[11] Chen, S., and Doolen, G., 1998, "Lattice Boltzmann Method for Fluid Flows," Ann. Rev. Fluid Mech., **30**, pp. 329–364.

[12] Succi, S., 2001, *The Lattice Boltzmann Equation for Fluid Dynamics and Beyond*, Clarendon, Oxford, UK.

[13] Luo, L.-S., 2000, "Theory of the Lattice Boltzmann Method: Lattice Boltzmann Models for Nonideal Gases," Phys. Rev. E, **62**, pp. 4982–4996.

[14] He, X., and Doolen, G., 2002, "Thermodynamic Foundations of Kinetic Theory and Lattice Boltzmann Models for Multiphase Flows," J. Stat. Phys., **107**, pp. 309–328.

[15] Asinari, P., 2006, "Semi-Implicit-Linearized Multiple-Relaxation-Time Formulation of Lattice Boltzmann Schemes for Mixture Modeling," Phys. Rev. E, **73**, p. 056705.

[16] Junk, M., Klar, A., and Luo, L.-S., 2005, "Asymptotic Analysis of the Lattice Boltzmann Equation," J. Comput. Phys., **210**, pp. 676–704.

[17] Bhatnagar, P. L., Gross, E., and Krook, M., 1954, "A Model for Collision Processes in Gases. I. Small Amplitude Processes in Charged and Neutral One-Component Systems," Phys. Rev., **94**, pp. 511–525.

[18] Qian, Y., d'Humières, D., and Lallemand, P., 1992, "Lattice BGK Models for Navier–Stokes Equation," Europhys. Lett., **17**, pp. 479–484.

[19] Chen, H., Chen, S., and Matthaeus, W. H., 1992, "Recovery of the Navier–Stokes Equations Using the Lattice-Gas Boltzmann Method," Phys. Rev. A, **45**, pp. R5339–R5342.

[20] d'Humières, D., 1992, "Generalized Lattice Boltzmann Equations," *Rarefied Gas Dynamics: Theory and Simulations, Progress in Aeronautics and Astronautics*, Vol. 159, B. D. Shigal, and D. P. Weaver, eds., AIAA, Washington, DC, pp. 450–458.

[21] Lallemand, P., and Luo, L.-S., 2000, "Theory of the Lattice Boltzmann Method: Dispersion, Dissipation, Isotropy, Galilean Invariance, and Stability," Phys. Rev. E, **61**, pp. 6546–6562.

[22] d'Humières, D., Ginzburg, I., Krafczyk, M., Lallemand, P., and Luo, L.-S., 2002, "Multiple-Relaxation-Time Lattice Boltzmann Models in Three Dimensions," Philos. Trans. R. Soc. London, Ser. A, **360**, pp. 437–451.

[23] Premnath, K. N., and Abraham, J., 2007, "Three-Dimensional Multi-Relaxation Time (MRT) Lattice-Boltzmann Models for Multiphase Flow," J. Comput. Phys., **224**, pp. 539–559.

[24] Pattison, M. J., Premnath, K. N., Morley, N. B., and Abdou, M. A., 2008, "Progress in Lattice Boltzmann Methods for Magnetohydrodynamic Flows Relevant to Fusion Applications," Fusion Eng. Des., **83**, pp. 557–572.

[25] Premnath, K. N., Pattison, M. J., and Banerjee, S., 2009, "Generalized Lattice Boltzmann Equation With Forcing Term for Computation of Wall Bounded Turbulent Flows," Phys. Rev. E, **79**, p. 026703.

[26] Ginzbourg, I., and Adler, P. M., 1994, "Boundary Flow Condition Analysis for the Three-Dimensional Lattice Boltzmann Model," J. Phys. II, **4**, pp. 191–214.

[27] Ginzburg, I., and d'Humieres, D., 2003, "Multireflection Boundary Conditions for Lattice Boltzmann Models," Phys. Rev. E, **68**, p. 066614.

[28] Pan, C., Luo, L.-S., and Miller, C. T., 2006, "An Evaluation of Lattice Boltzmann Schemes for Porous Medium Flow Simulation," Comput. Fluids, **35**, pp. 898–909.

[29] Luo, L.-S., Liao, W., Chen, X., Peng, Y., and Zhang, W., 2011, "Numerics of the Lattice Boltzmann Method: Effects of Collision Models on the Lattice Boltzmann Simulations," Phys. Rev. E, **83**, p. 056710.

[30] Ladd, A. J. C., and Verberg, R., 2001, "Lattice-Boltzmann Simulations of Particle-Fluid Suspensions," J. Stat. Phys., **104**, pp. 1191–1251.

[31] Succi, S., Karlin, I., and Chen, H., 2002, "Role of the H Theorem in Lattice Boltzmann Hydrodynamic Simulations," Rev. Mod. Phys., **74**, pp. 1203–1220.

[32] Yu, D., Mei, R., Luo, L.-S., and Shyy, W., 2003, "Viscous Flow Computations With the Method of Lattice Boltzmann Equation," Prog. Aerosp. Sci., **39**, pp. 329–367.

[33] Nourgaliev, R. R., Dinh, T. T., Theofanous, T. G., and Joseph, D., 2003, "The Lattice Boltzmann Equation Method: Theoretical Interpretation, Numerics and Implications," Int. J. Multiphase Flow, **29**, pp. 117–169.

[34] Premnath, K. N., McCracken, M. E., and Abraham, J., 2005, "A Review of Lattice Boltzmann Methods for Multiphase Flows Relevant to Engine Sprays," SAE, Technical Paper No. 2005-01-0996.

[35] Aidun, C., and Clausen, J. R., 2010, "Lattice-Boltzmann Method for Complex Flows," Ann. Rev. Fluid Mech., **42**, pp. 439–472.

[36] Luo, L.-S., Krafczyk, M., and Shyy, W., 2010, "Lattice Boltzmann Method for Computational Fluid Dynamics," *Encyclopedia of Aerospace Engineering*, pp. 651–660.

[37] Ansumali, S., Karlin, I., and Succi, S., 2004, "Kinetic Theory of Turbulence Modelling: Smallness Parameter, Scaling and Microscopic Derivation of Smagorinsky Model," Physica A, **338**, pp. 379–394.

[38] Chen, H., Orszag, S., Staroselsky, I., and Succi, S., 2004, "Expanded Analogy Between Boltzmann Kinetic Theory of Fluids and Turbulence," J. Fluid Mech., **519**, pp. 301–314.

[39] Malaspinas, O., and Sagaut, P., 2012, "Consistent Subgrid Scale Modelling for Lattice Boltzmann Methods," J. Fluid Mech., **700**, pp. 514–542.

[40] Chen, H., Kandasamy, S., Orszag, S., Shock, R., Succi, S., and Yakhot, V., 2003, "Extended Boltzmann Kinetic Equation for Turbulent Flows," Science **301**, pp. 633–636.

[41] Smagorinsky, J., 1963, "General Circulation Experiments With the Primitive Equations," Mon. Weather Rev., **91**, pp. 99–164.

[42] Hou, S., Sterling, J., Chen, S., and Doolen, G. D., 1996, "A Lattice Boltzmann Subgrid Model for High Reynolds Number Flows," *Pattern Formation and Lattice Gas Automata*, A. T. Lawniczak, and R. Kapral, eds., American Mathematical Society, Providence, RI, pp. 151–166.

Downloaded From: https://fluidsengineering.asmedigitalcollection.asme.org on 06/30/2019 Terms of Use: http://www.asme.org/about-asme/terms-of-use

[43] Krafczyk, M., Tolke, J., and Luo, L.-S., 2003, "Large-Eddy Simulations With a Multiple-Relaxation-Time LBE Model," Int. J. Mod. Phys. B, **17**, pp. 33–39.
[44] Yu, H., Luo, L.-S., and Girimaji, S., 2006, "LES of Turbulent Square Jet Flow Using an MRT Lattice Boltzmann Model," Comput. Fluids, **35**, pp. 957–965.
[45] van Driest, E., 1956, "On Turbulent Flow Near a Wall," J. Aeronaut. Sci., **23**, pp. 1007–1011.
[46] Dong, Y.-H., Sagaut, P., and Marie, S., 2008, "Inertial Consistent Subgrid Model for Large-Eddy Simulation Based on the Lattice Boltzmann Method," Phys. Fluids, **20**, p. 035104.
[47] Weickert, M., Teike, G., Schmidt, O., and Sommerfeld, M., 2010, "Investigation of the LES WALE Turbulence Model Within the Lattice Boltzmann Framework," Comput. Math. Appl., **59**, pp. 2200–2214.
[48] Stiebler, M., Krafczyk, M., Freudiger, S., and Geier, M., 2011, "Lattice Boltzmann Large Eddy Simulation of Subcritical Flows Around a Sphere on Non-Uniform Grids," Comput. Math. Appl., **61**, pp. 3475–3484.
[49] Freitas, R. K., Henze, A., Meinke, M., and Schröder, W., 2011, "Analysis of Lattice-Boltzmann Methods for Internal Flows," Comput. Fluids, **47**, pp. 115–121.
[50] Germano, M., Piomelli, U., Moin, P., and Cabot, W., 1991, "A Dynamic Subgrid-Scale Eddy Viscosity Model," Phys. Fluids A, **3**, pp. 1760–1765.
[51] Premnath, K. N., Pattison, M. J., and Banerjee, S., 2009, "Dynamic Subgrid Scale Modeling of Turbulent Flows Using Lattice-Boltzmann Method," Physica A, **388**, pp. 2640–2658.
[52] Wu, H., Wang, J., and Tao, Z., 2011, "Passive Heat Transfer in a Turbulent Channel Flow Simulation Using Large Eddy Simulation Based on the Lattice Boltzmann Method Framework," Int. J. Heat Fluid Flow, **32**, pp. 1111–1119.
[53] Qian, Y. H., Succi, S., Massaioli, F., and Orszag, S. A., 1996, "A Benchmark for Lattice BGK Model: Flow Over a Backward-Facing Step," *Pattern Formation and Lattice Gas Automata*, A. T. Lawniczak, and R. Kapral, eds., American Mathematical Society, Providence, RI, pp. 207–215.
[54] Chapman, S., and Cowling, T. G., 1964, *Mathematical Theory of Nonuniform Gases*, Cambridge University, Cambridge, England.
[55] Lilly, D., 1992, "A Proposed Modification of the Germano Subgrid-Scale Closure Method," Phys. Fluids A, **4**, pp. 633–635.
[56] He, X., Luo, L.-S., and Dembo, M., 1996, "Some Progress in the Lattice Boltzmann Method—Part 1: Non-Uniform Mesh Grids," J. Comput. Phys., **129**, pp. 357–363.
[57] Filippova, O., and Hänel, D., 1998, "Grid Refinement for Lattice-BGK Models," J. Comput. Phys., **147**, pp. 219–228.
[58] Yu, D., Mei, R., and Shyy, W., 2002, "A Multi-Block Lattice Boltzmann Method for Viscous Fluid Flows," Int. J. Numer. Methods Fluids, **39**, pp. 99–120.
[59] Chen, H., Filippova, O., Hoch, J., Molvig, K., Shock, R., Teixeira, C., and Zhang, R., 2006, "Grid Refinement in Lattice Boltzmann Methods Based on Volumetric Formulation," Physica A, **362**, pp. 158–167.
[60] Rohde, M., Kandhai, D., Derksen, J. J., and van den Akker, H. E. A., 2006, "A Generic, Mass Conservative Local Grid Refinement Technique for Lattice-Boltzmann Schemes," Int. J. Numer. Methods Fluids, **51**, pp. 439–468.
[61] Dupuis, A., and Chopard, B., 2003, "Theory and Applications of an Alternative Lattice Boltzmann Grid Refinement Algorithm," Phys. Rev. E, **67**, p. 066707.
[62] Rohde, M., Derksen, J. J., and van den Akker, H. E. A., 2008, "An Applicability Study of Advanced Lattice-Boltzmann Techniques for Moving, No-Slip Boundaries and Local Grid Refinement," Comput. Fluids, **37**, pp. 1238–1252.
[63] Spalart, P. R., 1987, "Direct Simulation of a Turbulent Boundary Layer Up to $R_\theta = 1410$," J. Fluid Mech., **187**, pp. 61–98.
[64] Ladd, A. J. C., 1994, "Numerical Simulations of Particulate Suspensions via a Discretized Boltzmann Equation—Part 1: Theoretical Foundation," J. Fluid Mech., **271**, pp. 285–309.
[65] Dubois, F., Lallemand, P., and Tekitek, M., 2010, "On a Superconvergent Lattice Boltzmann Boundary Scheme," Comput. Math. Appl., **59**, pp. 2141–2149.
[66] Pope, S., 2000, *Turbulent Flows*, Cambridge University, Cambridge, England.
[67] Gullbrand, J., and Chow, F. K., 2003, "The Effect of Numerical Errors and Turbulence Models in Large-Eddy Simulations of Channel Flow, With and Without Explicit Filtering," J. Fluid Mech., **495**, pp. 323–341.
[68] Lee, S., Lele, S. K., and Moin, P., 1992, "Simulation of Spatially Evolving Turbulence and the Applicability of Taylor's Hypothesis in Compressible Flow," Phys. Fluids, **4**, pp. 1521–1530.
[69] Batten, P., Goldberg, U., and Chakravarty, S., 2004, "Interfacing Statistical Turbulence Closures With Large-Eddy Simulation," AIAA J., **42**, pp. 485–492.
[70] Keating, A., Piomelli, U., Balaras, E., and Kaltenbach, H.-J., 2004, "*A Priori* and *a Posteriori* Tests of Inflow Conditions for Large-Eddy Simulation," Phys. Fluids, **16**, pp. 4696–4712.
[71] Lund, T. S., Wu, X., and Squires, K. D., 1998, "Generation of Inflow Data for Spatially Developing Boundary Layer Simulations," J. Comput. Phys., **140**, pp. 233–258.
[72] Spille–Kohoff, A., and Kaltenbach, H.-J., 2001, "Generation of Turbulent Inflow Data With a Prescribed Shear-Stress Profile," 3rd AFOSR International Conference on DNS/LES, C. Liu, L. Sakell, and T. Beutner, eds., Greyden Press, Columbus, OH.
[73] Terracol, M., 2006, "A Zonal RANS/LES Approach for Noise Sources Prediction," Flow, Turbul. Combust., **77**, pp. 161–184.
[74] Sandham, N. D., Yao, Y. F., and Lawal, A. A., 2003, "Large-Eddy Simulation of Transonic Turbulent Flow Over a Bump," Int. J. Heat Fluid Flow, **24**, pp. 584–595.
[75] Liu, M., Chen, X.-P., and Premnath, K. N., 2012, "Comparative Study of the Large Eddy Simulations With the Lattice Boltzmann Method Using the Wall-Adapting Local Eddy-Viscosity and Vreman Subgrid Scale Models," Chinese Phys. Lett., **29**, p. 104706.
[76] Nicoud, F., and Ducros, F., 1999, "Subgrid-Scale Stress Modelling Based on the Square of the Velocity Gradient Tensor," Flow, Turbul. Combust., **62**, pp. 183–200.

Downloaded From: https://fluidsengineering.asmedigitalcollection.asme.org on 06/30/2019 Terms of Use: http://www.asme.org/about-asme/terms-of-use